CHAPTER

# 9 SIMULATOR

For further research and development of the NR physical layer, we complement this book with a MATLAB-based link level simulator. We shall present an open-source simulator, including several waveforms, i.e., cyclic prefix based orthogonal frequency division multiplexing (CP-OFDM), windowed-OFDM (W-OFDM), universal filtered OFDM (UF-OFDM), discrete Fourier transform spread OFDM (DFTS-OFDM), offset QAM filter-bank multicarrier (FBMC-OQAM), and QAM filter-bank multicarrier (FBMC-QAM), various hardware impairments, i.e., power amplifier (PA) nonlinearity, oscillator phase noise (PN), and carrier frequency offset (CFO), and a geometry-based stochastic channel model supporting millimeter-wave channel emulation up to 80 GHz.

The simulator is developed by Qamcom Research & Technology AB. We release it with this book as an open-source simulator (with permission from Qamcom Research & Technology AB). The simulator can be accessed at **www.qamcom.se/research/5gsim**.

The simulator was originally developed in the EU funded mmMAGIC project [15] to assess performance of various waveforms in a common environment. As discussed in Chapter 5, several waveforms were proposed for 5G NR. Due to lack of a common waveform simulator, sometimes contradictory results were observed. Therefore, the mmMAGIC project realized importance of a transparent simulator for fair comparisons. Furthermore, the simulator was used to develop receiver algorithms for NR. At present (August 2018), the simulator has the following key components:

- A channel model up to 80 GHz (discussed in Chapter 3);
- A phase-noise model for a free-running oscillator and a phase-noise model for a phased-lock loop based oscillator (discussed in Chapter 4);
- A power-amplifier model based on a generalized memory polynomial (discussed in Chapter 4);
- Modulation/demodulation modules for various waveforms (discussed in Chapter 5);
- Algorithms for channel estimation & equalization, synchronization, and phase-noise compensation (discussed in Chapter 6).

It is likely that the simulator will evolve in the future with contributions from the authors and the open-source community.

This chapter is organized as follows. Section 9.1 provides an overview of the simulator, followed by details of different functional modules and waveforms in Section 9.2 and Section 9.3, respectively. Our ambition is not to discuss fundamentals (which are already covered in previous chapters); rather the focus is on implementation specific details. Finally, Section 9.4 shows a number of simulation exercises with various waveforms subject to the above-mentioned impairments and receiver algorithms. With these exercises, important observations are made.

**5G Physical Layer.** https://doi.org/10.1016/B978-0-12-814578-4.00014-X

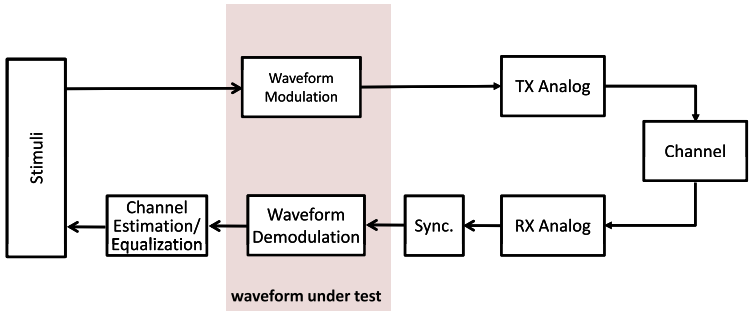


**FIGURE 9.1**

Block diagram of the simulator.

## 9.1 SIMULATOR OVERVIEW

A functional diagram of the simulator is shown in Fig. 9.1. The stimuli module sends (receives) QAM symbols to be modulated (demodulated) by the waveform modulator (demodulator). The modulated signal goes through analog modules at the transmitter (Tx) and receiver (Rx), and the radio channel. The Tx analog module adds hardware impairments, such as power amplifier (PA) nonlinearity, oscillator phase noise (PN), and carrier frequency offset (CFO) to the transmitted signal. The transmitted signal then experiences delay spread, Doppler spread, and interference, incurred by the channel model. After the radio channel, the received signal is further impaired by additive white Gaussian noise (AWGN) and PN that occur in the Rx analog module (before demodulation). At the receiver, timing and frequency synchronization are performed first. The synchronized signal is transformed to the frequency (subcarrier) domain by the waveform demodulator. Channel estimation and equalization are performed afterwards. (Note that it is possible to estimate the channel in the time domain before waveform demodulation. Nevertheless, the conventional frequency-domain channel estimation is chosen in this simulator.) At the moment, included waveforms are cyclic prefix (CP) based orthogonal frequency division multiplexing (OFDM) [5], windowed-OFDM (W-OFDM) [20], universal filtered OFDM (UF-OFDM) [22], discrete Fourier transform spread OFDM (DFT-S-OFDM) [4], offset QAM filter-bank multicarrier (FBMC-OQAM) [21], and QAM filter-bank multicarrier (FBMC-QAM) [17]. Other waveforms can be integrated into the open-source simulator as well.

We describe each module of the simulator separately in the following sections. Exemplary simulations are conducted to compare different waveforms and to illustrate the functionality of the simulator.

## 9.2 FUNCTIONAL MODULES

We present all the functional modules (except for waveforms) of the simulator separately in this section. The presentation of different waveforms is deferred to the next section.

### 9.2.1 CHANNEL MODEL

Both geometry-based channel models and 5G stochastic channel models [11–16] have been discussed in Chapter 2. Among the 5G stochastic channel model, the mmMAGIC (also known as QuaDRiGa) channel model [16] is the only one that has been made open-source. Therefore, we integrate the mmMAGIC channel model into the simulator. For the sake of completeness, we briefly present the mmMAGIC channel model here. The mmMAGIC channel model is an extension of the well-known WINNER channel model [1]. While the WINNER model is valid up to 6 GHz, the current version of the mmMAGIC channel model supports millimeter-wave channel up to 80 GHz. In addition, the mmMAGIC channel model can well predict the time variance of the channel (as compared to the WINNER model). The data flow of the mmMAGIC channel model is given as follows:

- define network layout, terminal trajectories, propagation scenarios along the trajectories, and antenna patterns of the terminals and base stations;
- calculate the maps of large-scale parameters (i.e., RMS delay spread, Rician $K$-factor, shadow fading, azimuth spread of departure/arrival, elevation spread of departure/arrival);
- calculate the initial delays, the path powers, and the angles of departure/arrival;
- calculate the polarized channel coefficients including the transmission loss, the shadow fading, and the $K$-factor.

A detailed description of the channel model can be found in [14]. The channel model can be switched off, in which case the channel boils down to a simple AWGN channel. This can be useful if one is only interested in making manifest the effect of a certain hardware impairment.

### 9.2.2 POWER AMPLIFIER MODEL

As discussed in Chapter 4, the PA effects can be accurately modeled by the Volterra series. Nevertheless, the Volterra series model can be quite complicated. By ignoring all the memory and crossterms, the Volterra series model boils down to the polynomial model. The polynomial model is very simple and allows analytical study. However, it cannot capture the dynamic or memory effect of the PA. As a trade-off, the memory polynomial and the generalized memory polynomial are introduced in modeling the PA effects. The former omits all the crossterms and, therefore, captures only the first degree of dynamic effects, whereas the latter only ignores part of the crossterms and is very close to the Volterra series model. The generalized memory polynomial (GMP) model is a good compromise between accuracy and complexity. As the nonlinear order increases, the variances of the estimated parameters also increases. To overcome this problem, local basis functions are used. Specifically, a vector-switched GMP (VS-GMP)-based PA model [2] is included in the simulator. The interested reader may refer to [2] for a detailed description of the PA model.

Note that the PA nonlinearity causes spectral regrowth, i.e., power leakage to adjacent channels or increased out-of-band (OOB) emissions. In order to correctly examine the PA effects, interpolation and decimation ought to be performed before and after the PA model. The implemented PA model [2] requires an interpolation with an oversampling factor of 5 to 7. Otherwise, the OOB emissions caused by the PA will incur a (nonphysical) inband distortion due to the spectral periodicity of time-discrete signals. The Parks–McClellan FIR filter [13] is used as anti-aliasing filter in the interpolation and decimation. Even though the Parks–McClellan FIR filter is close to an ideal low-pass filter, there will inevitably be some distortion in the transition around the cut-off frequency. As a result, guard bands

(i.e., zero subcarriers in the beginning and end of each multicarrier symbol) [10] are needed. The Parks–McClellan FIR filter has another effect: delaying the signal by half of the filter length. Since it is used twice (i.e., before and after the PA model), the filter delay equals its filter length. The filter delay and the delay caused by the random multipath channel will be estimated in the synchronization module.

The PA model can be switched off, in which case the Parks–McClellan FIR filter will be switched off automatically.

### 9.2.3 PHASE-NOISE MODEL

The PN of an oscillator is a multiplicative noise. It causes a random phase rotation of the received signal. For a multicarrier waveform, the PN causes common phase error (CPE) and inter-carrier interference (ICI). While the former represents a common phase rotation to all the subcarrier, the latter refers to the interference for each subcarrier caused by all the other ones. The CPE can be readily corrected using scattered pilots, whereas the ICI may be difficult to eliminate. There are ICI correction algorithms, e.g., [19], [7], which can effectively mitigate the ICI effect. However, these algorithms are computationally heavy.

As discussed in Chapter 3, the PN of a free-running oscillator can be modeled by a random walk (or Wiener) process, whose discrete-time expression is given by $\varphi(n+1) = \varphi[n] + w[n]$, where $\varphi$ is the PN and $w$ is a zero-mean Gaussian random variable whose variance is $4\pi\beta/f_s$ with $f_s$ denoting the sampling frequency and $\beta$ representing the 3-dB bandwidth of the phase noise. The Wiener PN model is perhaps the most popular PN model in the literature due to its simplicity and well-known statistical properties. However, its variance increases linearly with time. Hence, in practice, a phase-locked loop (PLL) is usually added to regularize the PN. A PN model of the PLL-based oscillator has been proposed in mmMAGIC [12]. This model was developed specifically for millimeter-wave communications. It is a more realistic (yet complicated) model as compared with the simple Wiener PN model. The PLL PN model is briefly mentioned in Chapter 3.

Both PN models are included in the simulator. The parameter $\beta$ is used to specify the quality of the free-running oscillator. The PLL PN model involves many parameters. For simplicity, "low" and "high" PN modes were implemented for good and bad PLL-based oscillators. The detailed modeling parameters of the PN of the PLL-based oscillator are listed in Table 9.1.

Either PN model can be chosen at the transmitter and the receiver. The PN model at either side can be switched on and off independently.

### 9.2.4 SYNCHRONIZATION

As mentioned before, the multipath channel and the filters will cause delay (timing offset) of the received signal. The timing offset has to be estimated before further processing of the received signal. The CFO represents the frequency difference between the carrier frequencies at the transmitter and at the receiver. If left uncompensated, it will cause a phase rotation of the received signal and the phase increases linearly with time. The synchronization module performs timing and frequency synchronization. By assuming common preamble, the timing offset, and CFO are estimated using the methods in [24] and [23], respectively. One can also choose perfect timing and frequency synchronization. In the former case, the true value of the timing offset is used for timing synchronization. In the latter case, the CFO is set to zero and the frequency synchronization module is disabled (since perfect frequency synchronization results in a CFO-free signal).

**Table 9.1 Parameter of "low" and "high" phase-noise settings**

| Component | Parameter | Value ($f_c$ is the carrier frequency in GHz) | |
|---|---|---|---|
| | | **Low** | **High** |
| Reference | $S_0$ | $-60+20log_{10}(f_c)$ (dBc/Hz) | $-60+20log_{10}(f_c)$ (dBc/Hz) |
| | $f_p$ | 1 Hz | 1 Hz |
| | $f_x$ | 10 kHz | 3980 Hz |
| PLL | $S_0$ | $-140.35+20log_{10}(f_c)$ (dBc/Hz) | $-122.35+20log_{10}(f_c)$ (dBc/Hz) |
| | $f_p$ | $\infty$ | $\infty$ |
| | $f_p$ | $\infty$ | $\infty$ |
| | $f_{fc}$ (flicker corner) | 2 MHz | 0.8 MHz |
| | $k$ (flicker exponent) | 1 | 1 |
| | $f_{fp}$ (flicker pole) | 200 Hz | 80 Hz |
| VCO | $S_0$ | $-24.34+20log_{10}(f_c)$ (dBc/Hz) | $-3.35+20log_{10}(f_c)$ (dBc/Hz) |
| | $f_p$ | 1 Hz | 1 Hz |
| | $f_x$ | 20 MHz | 80 MHz |
| Transfer function from reference and loop noise to output | $\frac{K_D K_{VCO} Z(s)}{sN_D+K_D K_{VCO} Z(s)}$ | $6.366\times10^{-7}s+1$ (Numerator) | $1.592\times10^{-6}s+1$ (Numerator) |
| | | $7.076\times10^{-29}s^4+5.780\times10^{-21}s^3+1.013\times10^{-13}s^2+6.366\times10^{-7}s+1$ (Denominator) | $6.214\times10^{-20}s^3+6.333\times10^{-13}s^2+1.592\times10^{-6}s+1$ (Denominator) |
| Transfer function from reference and loop noise to output | $\frac{sN_D}{sN_D+K_D K_{VCO} Z(s)}$ | $7.076\times10^{-29}s^4+5.780\times10^{-21}s^3+1.013\times10^{-13}s^2$ (Numerator) | $6.214\times10^{-20}s^3+6.333\times10^{-21}s^3+1.013\times10^{-13}s^2$ (Numerator) |
| | | $7.076\times10^{-29}s^4+5.780\times10^{-21}s^3+1.013\times10^{-13}s^2+6.366\times10^{-7}s+1$ (Numerator) | $6.214\times10^{-20}s^3+6.333\times10^{-13}s^2+1.592\times10^{-6}s+1$ (Denominator) |

### 9.2.5 CHANNEL ESTIMATION AND EQUALIZATION

The frequency-domain channel estimation (equalization) is used in the simulator. The exact channel estimation methods may differ slightly for different waveforms. Yet, in essence, the channel transfer functions (CTFs) are estimated at the pilot subcarriers using the least-square (LS) estimator and the CTFs at other subcarriers are obtained by filtering [6].

Like the synchronization, the simulator allows for perfect channel estimation, in which case the true value of the channel transfer function is used for channel equalization.

## 9.3 WAVEFORMS

Several waveforms have been presented in Chapter 5. In the following subsections, we will briefly introduce these waveforms from an implementation point of view in the simulator. For all waveforms, the received (equivalent baseband) signal subject to phase noise, CFO, and multipath channel with

additive noise is modeled as

$$y[n] = \exp\left(j\left(\phi[n] + 2\pi\varepsilon n\right)\right) \sum_{l=0}^{L-1} h_l x[n-l-v] + w[n] \tag{9.1}$$

where $\varepsilon$ denotes the CFO (normalized by the sampling frequency), $\phi$ denotes the PN at the receiver, $x$ represents the transmitted time-domain signal, $h_l$ is the $l$th tap of the channel impulse response (CIR), $L$ denotes the channel length, and $w$ denotes the AWGN. Note that, for notational simplicity and without loss of generality, the effects of PA and PN at the transmitter have been omitted in the expression.

### 9.3.1 CP-OFDM

The CP-based OFDM (CP-OFDM) enjoys the simplest (de)modulation implementation among all the multicarrier waveforms. Its modulation can be expressed as

$$\mathbf{x} = [\mathbf{F}_{\mathrm{CP}}\ \mathbf{F}]^H\ \mathbf{s}, \tag{9.2}$$

where $\mathbf{s}$ denotes the $N \times 1$ column vector consisting of the subcarrier symbols, $\mathbf{F}$ denotes the $N \times N$ discrete Fourier transform (DFT) matrix whose element is given by $\exp(-j2\pi kn/N)/\sqrt{N}$ $(k, n = 0, \cdots, N-1)$, and $\mathbf{F}_{\mathrm{CP}}$ consists of the last $N_{\mathrm{CP}}$ columns of $\mathbf{F}$ (where $N_{\mathrm{CP}}$ denoting the CP length). Note that $\mathbf{F}_{\mathrm{CP}}\,\mathbf{s}$ forms the CP of the CP-OFDM symbol. The CP-OFDM demodulation matrix is given by $[\mathbf{0}\ \mathbf{F}]$, where $\mathbf{0}$ is an $N \times N_{\mathrm{CP}}$ zero matrix for CP removal.

### 9.3.2 W-OFDM

One can improve the OOB emission of the CP-OFDM by applying a windowing function to the transmitted time-domain signal, i.e., W-OFDM. Because of the windowing, the W-OFDM is also called weighted CP-OFDM (WCP-OFDM) [20]. By tapering the edges of the time-domain signal, the OOB emission can be reduced significantly. The tapering at the left edge causes no distortion of the useful signal thanks to the CP. To correct for the distortion due to the tapering at the right edge, the left edge of the received signal is added to the right edge, as explained in Chapter 5. This operation is called weighted overlap and add (WOLA) [9].

The raised-cosine filter is chosen as the windowing function in the simulator. The WOLA operation is implemented in the timing synchronization module at the W-OFDM receiver.

### 9.3.3 UF-OFDM

The UF-OFDM is also known as the universal filtered multicarrier (UFMC) [22]. It is achieved by first grouping the active subcarriers into $B$ blocks of consecutive subcarriers, and then performing inverse discrete Fourier transform (IDFT) and filtering to each of the blocks. For the sake of convenience in the implementation, each block contains $N_0$ subcarriers. The filter bank is obtained by exponential modulation of a prototype filter of length $N_{\mathrm{v}}$. The Dolph–Chebyshev filter is used as the prototype

filter in the simulator. The UF-OFDM modulation can be expressed as

$$\mathbf{x} = \sum_{i=1}^{B} \mathbf{V}_i \mathbf{D}_i \mathbf{s}_i \tag{9.3}$$

where the subscript $_i$ is the block index, $\mathbf{s}_i = [s_i(0), \cdots, s_i(N_0 - 1)]^T$ consists of symbols and scattered pilots to be modulated on the $N_0$ subcarriers in the $i$th block, $\mathbf{D}_i$ consists of $N_0$ columns corresponding the subcarriers in the $i$th block submatrix of the IDFT matrix $\mathbf{F}^H$, and $\mathbf{V}_i$ is a Toeplitz matrix whose first column vector is given by $[v_i(0), \cdots, v_i(N_\mathrm{v}), 0, \cdots, 0]^T$ where $v_i[n] = v[n]\exp(-j2\pi n k_i / N_\mathrm{v})$ with $k_i$ denoting the center frequency of the $i$th block and $v[n]$ denoting the $n$th tap of the prototype filter. The UF-OFDM demodulation can be achieved by performing $2N_\mathrm{f}$-point DFT of the zero-padded time-domain UF-OFDM symbol and then down sampling the frequency-domain signal by a factor of 2.

Note that a time-domain preprocessing has to be performed at the transmitter after the UF-OFDM modulation in order to remove the deterministic distortion introduced by the filter bank at the transmitter [22].

By performing filtering on groups of subcarriers, the OOB emission can be reduced significantly at the cost of increased complexity. There is also modest increase of symbol length due to the filters. Note that the performance of the UF-OFDM can be improved by introducing a CP in the presence of large delay spread [9] at the cost of increased overhead.

### 9.3.4 FBMC-OQAM

The FBMC-OQAM is also known as FBMC [3]. It applies a filter to each of the subcarriers. The filter length is $K$ times of the number of subcarriers. $K$ is the overlapping factor (which is a positive integer number). The filter bank can be implemented in the frequency domain using the frequency spreading method [3], which increases the DFT size from $N$ to $KN$. Since the IDFT output and DFT input are overlapped in the time domain, a significant amount of redundancy is present in the computations of the frequency spreading method. In order to reduce this redundancy, the simulator implements the FBMC-OQAM in the time domain using the polyphase network (PPN) method [3].

Unlike the CP-OFDM, the neighboring subcarriers of the FBMC-OQAM are overlapped. The imaginary part of the impulse response of the subcarrier interference filter crosses the time axis at the integer multiples of the symbol period and the real part crosses the time axis at the odd multiples of half the symbol period [3]. The OQAM can be used in combination of the FBMC to avoid subcarrier interference without sacrificing the spectral efficiency. Specifically, this is achieved by doubling the symbol rate and using alternatively the real and the imaginary part for each subchannel. The FBMC-OQAM has good frequency localization (e.g., very low OOB emission) and high spectral efficiency (i.e., no CP overhead). Nevertheless, the FBMC-OQAM suffers from high complexity and long delay, i.e., $K - 1/2$ symbol durations. Another drawback is that it is not directly compatible with MIMO systems due to the staggered OQAM.

In the simulator, we adopt the PHYDYAS prototype filter with an (integer) overlapping factor $K$ ranging from 2 to 4 [3]. A larger $K$ results in better frequency localization, yet higher complexity and longer delay.

### 9.3.5 FBMC-QAM

To avoid the inconvenience caused by the OQAM, the QAM-based FBMC (FBMC-QAM) with dual filter banks was proposed [18]. A prototype filter in one filter bank is obtained by block interleaving the prototype filter in the other filter bank. The FBMC-QAM modulator performs filtering for even and odd subcarriers separately. The proposed filter banks in [18] ensure orthogonal subcarriers yet has higher OOB emission than that of the CP-OFDM. As a tradeoff between low OOB emission and high signal-to-interference ratio (SIR), two types of filters were proposed in [25]. Generally speaking, filters with lower OOB emission will result in lower SIR. The filter type I has a spectrum similar to that of the FBMC-OQAM with PHYDYAS filter (i.e., good frequency localization) yet poor SIR (10.6 dB). The filter type II has a wider spectrum, yet 9-dB higher SIR (19.6 dB) [25].

Like the FBMC-OQAM, the FBMC-QAM enjoys a high spectral efficiency (i.e., there is no CP overhead), yet suffers from high complexity and long delay. Unlike the FBMC-OQAM, the FBMC-QAM is compatible with MIMO systems at the cost of degradations in SIR and/or OOB emission.

In the simulator, the two types of filters in [25] and the filters in [18] are implemented for a fixed overlapping factor of $K = 4$. They are referred to as filter type I, II, and III, respectively.

## 9.4 SIMULATION EXERCISES

In this section, we compare the performances of different waveforms using the simulator. The simulator is written using object-oriented programming in MATLAB. To run the simulator, one needs to first direct to the subfolder **[.../waveformSimulator/ptplink]** in MATLAB. System parameters (waveform, symbol rate, subcarrier number, etc.) can be changed in a file named **sSysParDefault.m**. Different analog impairments (PN, CFO, AWGN, etc.) can be switched on and off in a file named **sAnaParDefault.m**. After all the parameters have been set, one needs to run **setpath.m** to add the paths of all the necessary folders. Finally, running **runSim.m**, it will perform simulation of the chosen waveform. Some simulation examples can be found in the subfolder **[.../ptplink/examples]**.

### 9.4.1 SPECTRAL REGROWTH

As mentioned in the previous section, certain waveforms (e.g., UF-OFDM and FBMC-OQAM) outperform the CP-OFDM in terms of OOB emissions (at the cost of increased complexity). Nevertheless, there can be spectral regrowth when waveforms are subject to PA nonlinearities. Here we show the spectral regrowths of CP-OFDM, UF-OFDM, W-OFDM, and FBMC-OQAM using the simulator.

The measurement setup is given below. We assume a DFT size of 512, out of which 158 are reserved as a guard band (i.e., 79 subcarriers in the beginning and end of each multicarrier symbol are set to zero), and QPSK modulation. In order to correctly include the OOB emission due to the PA nonlinearity, an interpolation with an oversampling factor of 5 and the Parks–McClellan optimal finite impulse response (FIR) filter as the anti-aliasing filter are used. For UF-OFDM modulation, we additionally assume Dolph–Chebyshev filter (with 64 filter taps and 40-dB stop band suppression) as the prototype filter and 16 subcarriers per filter. For W-OFDM modulation, we additionally assume a time-domain raised-cosine window (with 32 tapering length at the left and right soft edges). For FBMC-OQAM modulation, we assume an overlapping factor of 4 ($K = 4$) unless otherwise specified.

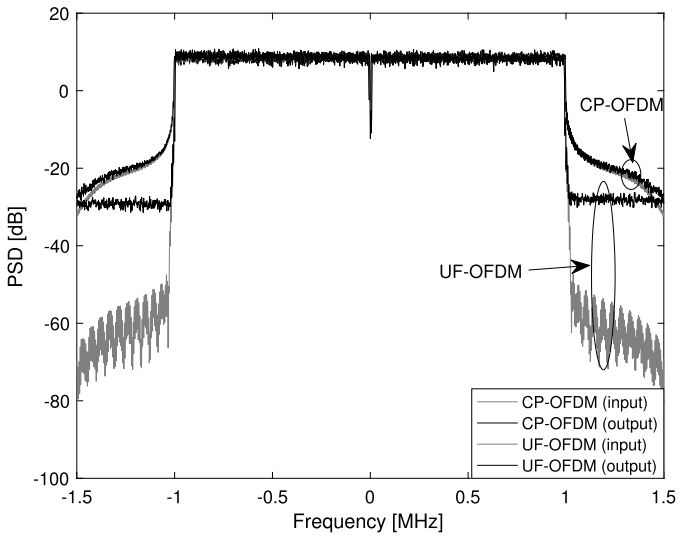


**FIGURE 9.2**

Spectral regrowths of CP- and UF-OFDM under PA nonlinearity: low input power (with 10-dB additional backoff).

Figs. 9.2–9.6 show the spectral regrowths of CP-, UF-, and W-OFDM under PA nonlinearities. As can be seen, the UF-OFDM has lower OOB emission as compared with the CP-OFDM, especially at low input power. Nevertheless, as the input power increases, the OOB emission of the UF-OFDM increases more than that of the CP-OFDM. That is, the OOB advantage of the UF-OFDM over the CP-OFDM diminishes at high input power. It is noted that the OOB emission of the CP-OFDM can be greatly improved by introducing a time-domain window to it, i.e., the W-OFDM. The OOB emissions of W- and UF-OFDM become comparable under PA nonlinearities. It is apparent that the FBMC-OQAM with an overlapping factor of 4 has much narrower OOB emission than the UF-OFDM does. Nevertheless, their spectra overlap under PA nonlinearities. It should also be noted that, in the absence of PA nonlinearities, the OOB emission of the FBMC-OQAM with an overlapping factor of 2 ($K = 2$) becomes larger than that with an overlapping factor of four (yet still smaller than that of the CP-OFDM). For the conciseness of the paper, the corresponding results are omitted here. All in all, it is shown that OOB emissions can be improved by filter banks; however, the improvements become insignificant when the PA nonlinearities are taken into account.

## 9.4.2 IMPAIRMENT OF CFO

The carrier frequencies generated by oscillators at the transmitter and the receiver are usually not identical. The difference between the two carrier frequency is referred to as the carrier frequency offset (CFO). The CFO destroys the orthogonality of multicarrier waveforms, resulting in performance degradations for different waveforms. In this exercise, we study the CFO impairment to different waveforms by simulations.

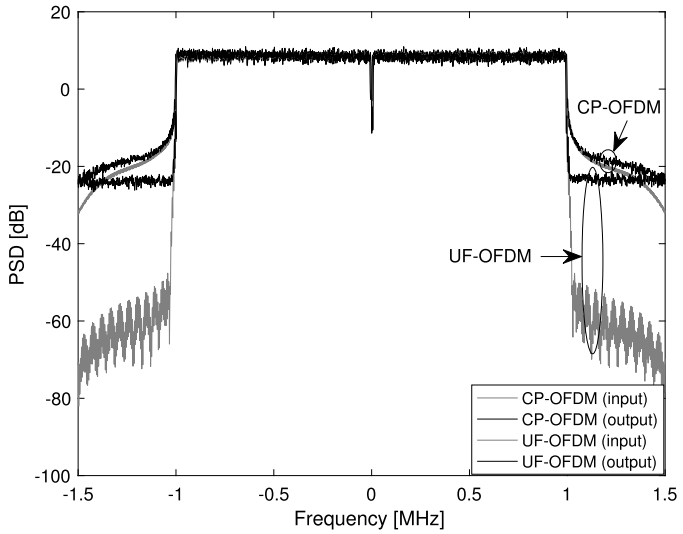


**FIGURE 9.3**

Spectral regrowths of CP- and UF-OFDM under PA nonlinearity: high input power.

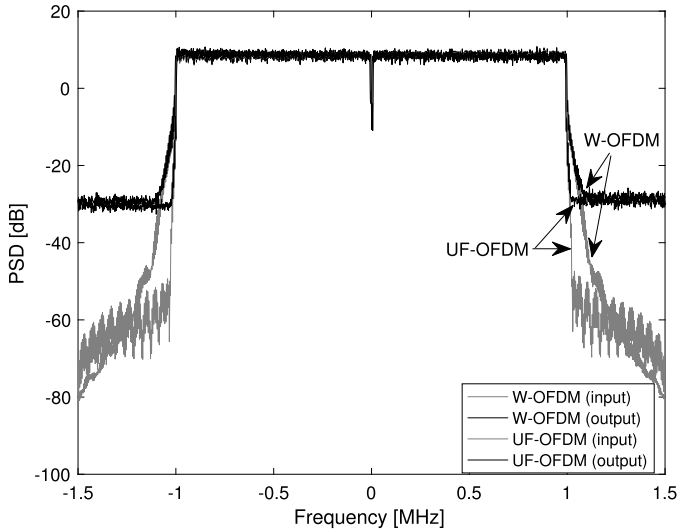


**FIGURE 9.4**

Spectral regrowths of W- and UF-OFDM with low input power.

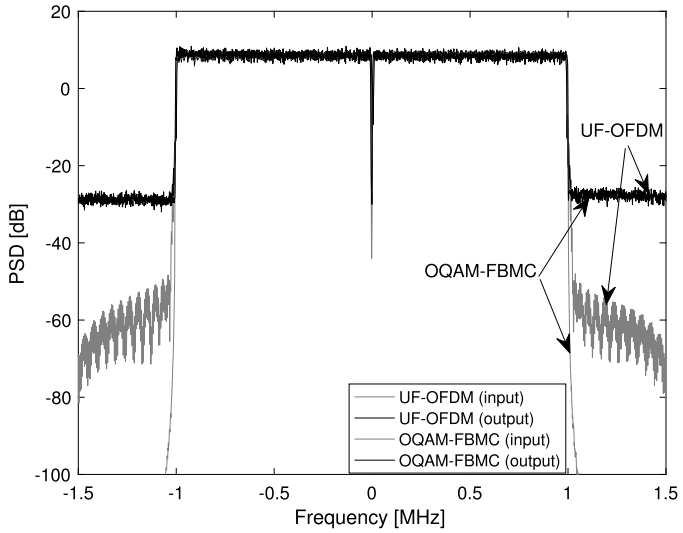


**FIGURE 9.5**

Spectral regrowths of UF-OFDM and FBMC-OQAM with low input power.

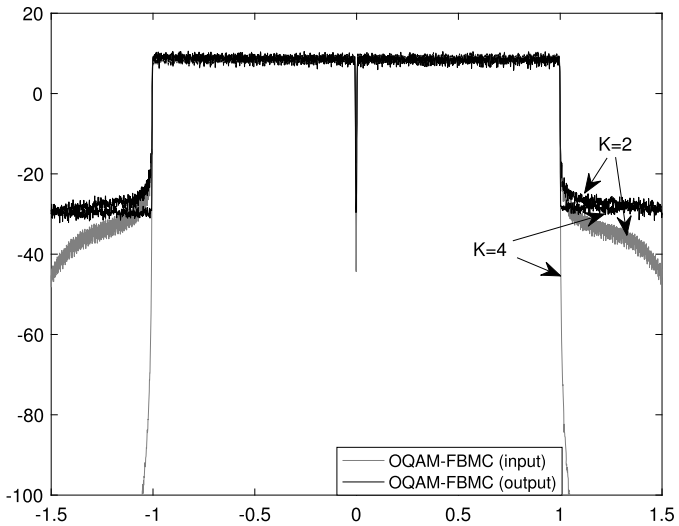


**FIGURE 9.6**

Spectral regrowths of FBMC-OQAM with different overlapping factors and low input power.

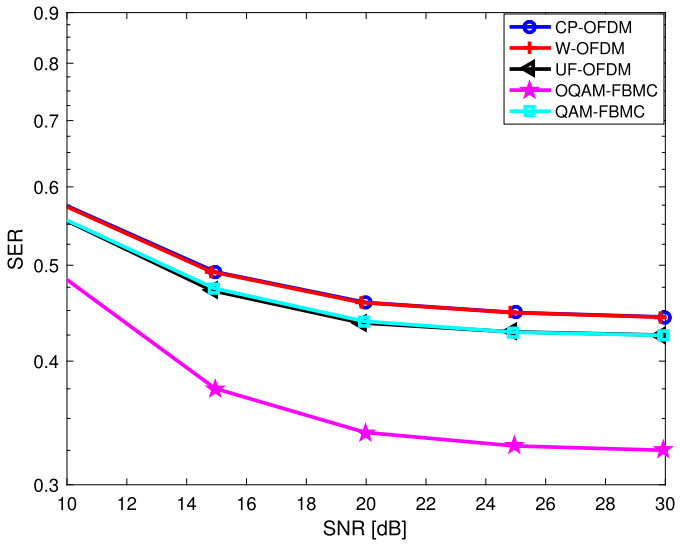


**FIGURE 9.7**

SER performances of different waveforms with 100 Hz CFO.

For fair comparisons of different waveforms, we disable the frequency synchronization module and assume 100 and 1000 Hz CFOs. In addition, we assume 1024 subcarriers, 100 MHz bandwidth, 16-QAM, and 100 multicarrier symbols. For the UF-OFDM, we assume the Dolph–Chebyshev filter (with 64 filter taps and 40-dB stop band suppression) as the prototype filter and 16 subcarriers per filter. For the W-OFDM, we assume a time-domain raised-cosine window with a tapering length of 32 at the left and right soft edges. For the FBMC-OQAM, we assume a PHYDYAS prototype filter with an overlapping factor of 4. For the FBMC-QAM, we assume the filter type II with an overlapping factor of 4 (cf. Section 9.3), since it is a good tradeoff between OOB emission and SIR [25]. In order to focus on the CFO effect, we ignore all the other hardware effects and assume an AWGN channel.

Fig. 9.7 and Fig. 9.8 show the symbol error rate (SER) performances of different waveforms under 100 and 1000 Hz CFOs, respectively. As can be seen, the FBMC-OQAM has the best SER performance and the UF-OFDM has the second best SER performance due to their filter bank. The SER performance of the FBMC-QAM depends on the value of the CFO and is no better than that of the UF-OFDM. The latter feature is because the filter type II in the FBMC-QAM is a compromise between OOB emission and SIR and because it does not guarantee orthogonality. Nevertheless, it should be noted that the SER improvements of the filter-bank-based waveforms (e.g., FBMC-OQAM and UF-OFDM) over that of the CP-OFDM tend to diminish (or become less significant) as the CFO increases.

As can be seen, without frequency synchronization, the system will not work. In practice, a coarse frequency synchronization (e.g., [23]) is performed prior to demodulation at the receiver. The residual CFO from the imperfect frequency synchronization can be further mitigated (together with the PN) using PN mitigation algorithms [8]. Since different waveforms apply different filters (which affect the signal powers of the waveforms), the exact SNR differs from the conventional $E_S/N_0$ (symbol energy

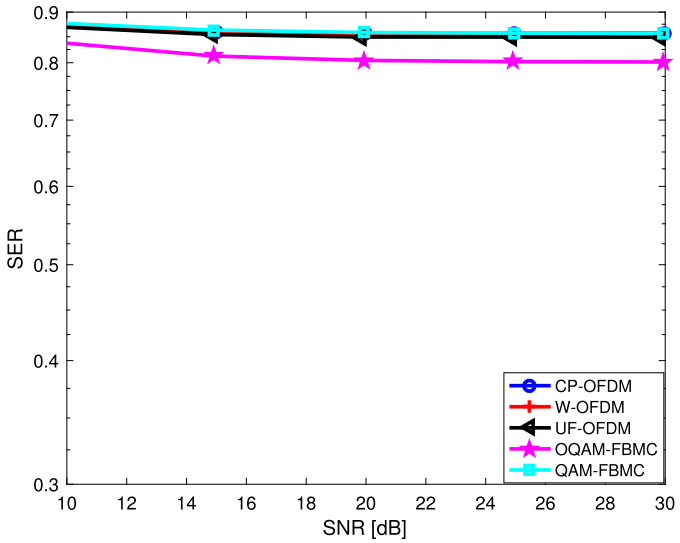


**FIGURE 9.8**

SER performances of different waveforms with 1000 Hz CFO.

over noise power density). As a result, we estimate the signal powers of different waveforms from their transmitted (time-domain) signals, respectively.

### 9.4.3 IMPAIRMENT OF PN

On top of the carrier frequency, the oscillator also produces random jitter frequency, which results in random PN. The PN causes random phase rotation of the signal and destroys the orthogonality of the multicarrier waveforms. In this exercise, we study the PN impairment to different waveforms by simulations.

As mentioned in Section 9.2.3, the PN effects in the frequency domain can be categorized as CPE and ICI. While the CPE can easily be estimated, the ICI is different to track. The advanced ICI correction algorithms (see, e.g., [19], [7]) are usually computationally expensive and waveform-specific, and may not always be feasible.

We assume perfect timing and frequency synchronization, 1024 subcarriers, 100 MHz bandwidth, 16-QAM, and 100 multicarrier symbols. For the UF-OFDM, we assume the Dolph–Chebyshev filter (with 64 filter taps and 40-dB stop band suppression) as the prototype filter and 16 subcarriers per filter. For the W-OFDM, we assume a time-domain raised-cosine window with 32 tapering length at the left and right soft edges. For the FBMC-OQAM, we use the PHYDYAS prototype filter with an overlapping factor of 4. For the FBMC-QAM, we assume the filter type II with an overlapping factor of four (cf. Section 9.3) since it is a good tradeoff between OOB emission and SIR [25]. In order to focus on the PN effect, we ignore all the other hardware effects and assume an AWGN channel.

Fig. 9.9 and Fig. 9.10 shows the SER performance of different waveforms in the presence of PN without and with CPE correction, respectively. As can be seen, the CPE corrections improve the SER

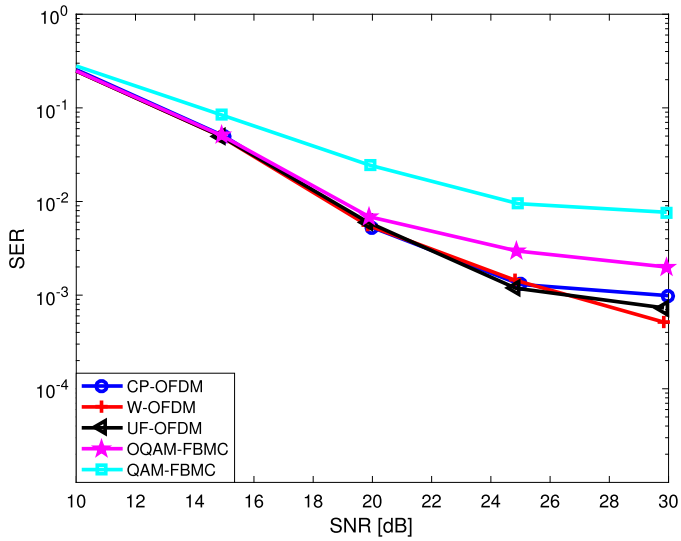


**FIGURE 9.9**

SER performances of different waveforms subject to PN without any receiver compensation.

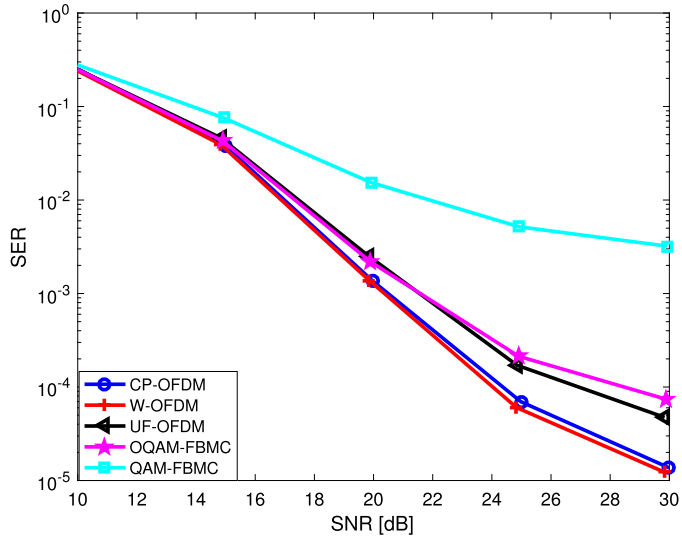


**FIGURE 9.10**

SER performances of different waveforms subject to PN with CPE correction.

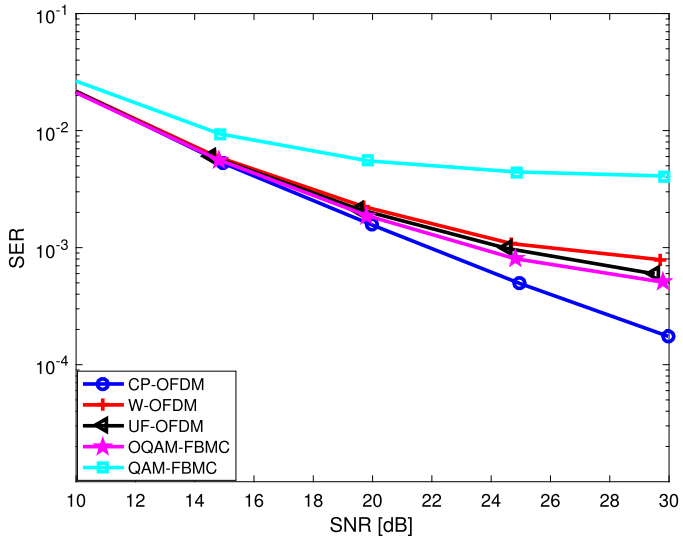


**FIGURE 9.11**

SER performances of different waveforms in time-varying fading channel with a user speed of 60 km/h at 6 GHz.

performances of the considered waveforms. Unlike the (constant) CFO, the PN arises from random jitter frequency. In this case, the W- and CP-OFDM have better SER performances than the other filter-bank-based waveforms, especially after the CPE removal. Due to the intrinsic SIR, the FBMC-QAM (with filter type II) has the worst SER performance under the PN.

### 9.4.4 IMPAIRMENT OF FADING CHANNEL

The multicarrier waveforms were introduced to cope with the multipath effect of the propagation channel in broadband communications. In this exercise, we compare SER performances of different waveforms in the multipath fading channel. We assume perfect timing and frequency synchronization, 512 subcarriers, 120 MHz bandwidth, and QAM. Like before, we assume the Dolph–Chebyshev filter (with 64 filter taps and 40-dB stop band suppression) as the prototype filter and 16 subcarriers per filter for UF-OFDM, a time-domain raised-cosine window with 32 tapering length at the left and right soft edges for W-OFDM, the PHYDYAS prototype filter with an overlapping factor of 4 for FBMC-OQAM, and the filter type II with an overlapping factor of 4 for FBMC-QAM. In order to focus on the multipath channel effect, we assume perfect channel estimation, ignore all the hardware effects, and resort to the QuaDRiGa channel model [16]. Unlike the WINNER channel model [1], the QuaDRiGa channel model can well emulate the time variation of the fading channel [14]. We assume a user speed of 60 km/h at 6 GHz. For each channel drop (realization), 50 multicarrier symbols were transmitted. In total, 60 channel drops were simulated. The SER performances of different waveforms are shown in Fig. 9.11. As can be seen, the CP-OFDM has the best SER performance in the time-varying fading channel; the FBMC-OQAM, UF-OFDM, and W-OFDM have similar SER performances; and the

FBMC-QAM has the worst SER performance. Note that the performance of the FBMC-QAM can be improved by using the type III filter at the expense of a higher OOB emission than the CP-OFDM [18].

## REFERENCES


[1] P. Kyosti, J. Meinila, L. Hentila, et al., IST-4-027756 WINNER II D1.1.2 V1.2 WINNER II Channel Models: Part I Channel Models, 2007.

[2] S. Afsardoost, T. Eriksson, C. Fager, Digital predistortion using a vector-switched model, IEEE Transactions on Microwave Theory and Techniques (ISSN 0018-9480) 60 (4) (2012, April) 1166–1174, https://doi.org/10.1109/TMTT.2012.2184295.

[3] M. Bellanger, et al., FBMC physical layer: a primer, http://www.ict-phydyas.org, 2010, 06.

[4] G. Berardinelli, Generalized DFT-S-OFDM waveforms without cyclic prefix, IEEE Access 6 (2018) 4677–4689, https://doi.org/10.1109/ACCESS.2017.2781122.

[5] J.A.C. Bingham, Multicarrier modulation for data transmission: an idea whose time has come, IEEE Communications Magazine (ISSN 0163-6804) 28 (5) (1990, May) 5–14, https://doi.org/10.1109/35.54342.

[6] X. Chen, A. Wolfgang, Phase noise mitigation in OFDM-based backhaul in the presence of channel estimation and synchronization errors, in: 2016 IEEE 83rd Vehicular Technology Conference (VTC Spring), 2016, May, pp. 1–5.

[7] X. Chen, S. Zhang, Antenna mutual coupling effect on MIMO-OFDM system in the presence of phase noise, in: 2017 11th European Conference on Antennas and Propagation (EUCAP), 2017, March, pp. 653–657.

[8] X. Chen, A. Wolfgang, A. Zaidi, MIMO-OFDM for small cell backhaul in the presence of synchronization errors and phase noise, in: 2017 IEEE International Conference on Communications Workshops (ICC Workshops), 2017, May, pp. 1221–1226.

[9] A. Daher, E.H. Baghious, G. Burel, E. Radoi, Overlap-save and overlap-add filters: optimal design and comparison, IEEE Transactions on Signal Processing (ISSN 1053-587X) 58 (6) (2010, June) 3066–3075, https://doi.org/10.1109/TSP.2010.2044260.

[10] M. Faulkner, The effect of filtering on the performance of OFDM systems, IEEE Transactions on Vehicular Technology (ISSN 0018-9545) 49 (5) (2000, Sep.) 1877–1884, https://doi.org/10.1109/25.892590.

[11] K. Guan, G. Li, T. Kurner, A.F. Molisch, B. Peng, R. He, B. Hui, J. Kim, Z. Zhong, On millimeter wave and THz mobile radio channel for smart rail mobility, IEEE Transactions on Vehicular Technology (ISSN 0018-9545) 66 (7) (2017, July) 5658–5674, https://doi.org/10.1109/TVT.2016.2624504.

[12] H2020-ICT-671650-mmMAGIC/D5.1 2016 mmMAGIC Deliverable D5.1. Initial multi-node and antenna transmitter and receiver architectures and schemes.

[13] S. Haykin, Adaptive Filter Theory, Prentice-Hall, 1996.

[14] F.H.H. Institute, Quasi deterministic radio channel generator user manual and documentation, document revision: v1.4.8-571, 2016, Sep.

[15] J. Luo, A.A. Zaidi, J. Vihriälä, D. Giustiniano, et al., Preliminary radio interface concepts for mm-wave mobile communications. Deliverable D4.1, Millimetre-Wave Based Mobile Radio Access Network for Fifth Generation Integrated Communications (mmMAGIC), https://5g-mmmagic.eu/results, 2016.

[16] S. Jaeckel, L. Raschkowski, K. Borner, L. Thiele, Quadriga: a 3-d multi-cell channel model with time evolution for enabling virtual field trials, IEEE Transactions on Antennas and Propagation (ISSN 0018-926X) 62 (6) (2014, June) 3242–3256, https://doi.org/10.1109/TAP.2014.2310220.

[17] C. Kim, K. Kim, Y.H. Yun, Z. Ho, B. Lee, J.Y. Seol, QAM-FBMC: a new multi-carrier system for post-ofdm wireless communications, in: 2015 IEEE Global Communications Conference (GLOBECOM), 2015, Dec., pp. 1–6.

[18] H. Nam, M. Choi, C. Kim, D. Hong, S. Choi, A new filter-bank multicarrier system for QAM signal transmission and reception, in: 2014 IEEE International Conference on Communications (ICC), 2014, June, pp. 5227–5232.

[19] D. Petrovic, W. Rave, G. Fettweis, Effects of phase noise on OFDM systems with and without pll: characterization and compensation, IEEE Transactions on Communications (ISSN 0090-6778) 55 (8) (2007, Aug.) 1607–1616, https://doi.org/10.1109/TCOMM.2007.902593.

[20] D. Roque, C. Siclet, Performances of weighted cyclic prefix OFDM with low-complexity equalization, IEEE Communications Letters (ISSN 1089-7798) 17 (3) (2013, March) 439–442, https://doi.org/10.1109/LCOMM.2013.011513.121997.

[21] P. Siohan, C. Siclet, N. Lacaille, Analysis and design of OFDM/OQAM systems based on filterbank theory, IEEE Transactions on Signal Processing (ISSN 1053-587X) 50 (5) (2002, May) 1170–1183, https://doi.org/10.1109/78.995073.

[22] V. Vakilian, T. Wild, F. Schaich, S. ten Brink, J.F. Frigon, Universal-filtered multi-carrier technique for wireless systems beyond LTE, in: 2013 IEEE Globecom Workshops (GC Wkshps), 2013, Dec., pp. 223–228.
[23] J.J. van de Beek, M. Sandell, P.O. Borjesson, Ml estimation of time and frequency offset in OFDM systems, IEEE Transactions on Signal Processing (ISSN 1053-587X) 45 (7) (1997, Jul.) 1800–1805, https://doi.org/10.1109/78.599949.
[24] G. Yi, L. Gang, G. Jianhua, A novel time and frequency synchronization scheme for OFDM systems, IEEE Transactions on Consumer Electronics (ISSN 0098-3063) 54 (2) (2008, May) 321–325, https://doi.org/10.1109/TCE.2008.4560093.
[25] Y.H. Yun, C. Kim, K. Kim, Z. Ho, B. Lee, J.Y. Seol, A new waveform enabling enhanced QAM-FBMC systems, in: 2015 IEEE 16th International Workshop on Signal Processing Advances in Wireless Communications (SPAWC), 2015, June, pp. 116–120.